tion or a regular phenomenon, etc.

The author has advanced the idea that each cosmic body with dimensions of a star always has a magnetic field in a rather tangled form. If the star has besides the tangled magnetic field also a regular one, then the latter originates from the tangled field by the rotation of the star.

The problem of the tangled magnetic field gives rise to the problem of the energy spectrum, or the problem of the distribution of the energy among the individual Fourier components of the field in a certain equilibrium state. Since the laws governing the tangled magnetic field correspond almost completely to the laws of turbulent motion of a viscous liquid, it is possible, by using the latter, to obtain the spectral law also for the case of interest to us. In the paper, however, the problem is solved by means of different ideas, which can lead to new aspects.

A high-temperature plasma can be represented as a mixture of ionized gas and a gas consisting of particles of electromagnetic radiation—photons. In the state of thermal equilibrium, there should exist photons of all wave-lengths, from the very shortest to the very longest and superlong ones, on the order of several dozen, hundreds, thousands of kilometers and more. On the other hand, in the case of an electrically conducting medium the superlong-wave electromagnetic radiation can no longer be represented by traveling waves, as can be done in a dielectric medium or in vacuum. From the corresponding analysis of Maxwell's equations it follows that superlong wave radiation in the case considered by us is expressed and represented by a tangled magnetic field which remains practically invariant in time. Thus, in the spectral representation, the magnetic field is a continuation of the spectrum of the ordinary electromagnetic radiation into the long-wave band. In a state of a certain, say thermal, equilibrium the tangled magnetic field is an organic part of the general spectrum of the electromagnetic radiation, and should always be present. We can therefore draw from this a new deduction, namely that the tangled magnetic field is a normal satellite of any star, just as the shorter-wavelength electromagnetic radiation.

The most general mechanism generating the weak primary field consists of the random fluctuations of the charges and electrons in the high-temperature plasma. Of course, these fluctuations are not the only causes of the magnetic field. In calculating the energy density of the superlong-wave part of the electromagnetic-radiation part in thermal equilibrium, it is not necessary to know the mechanism producing the magnetic field. It is only important to assume that the superlong wave radiation appears and that the principle of entropy increase is realized during a conceivable time interval. The spectral energy density is then calculated by the methods of thermodynamics and statistical physics.

If we disregard the motion of the medium, using the well-developed plasma theory, we can calculate the spectral distribution of the energy density of the superlong wave part of the electromagnetic radiation (the medium is assumed to be infinite):

$$E_\lambda\, d\lambda = \frac{1}{8\pi}\overline{H_\lambda^2}\, d\lambda = kT\frac{d\lambda}{\lambda^4}, \qquad (1)$$

where k is Boltzmann's constant, T is the temperature of the medium, λ is the wavelength of the Fourier component of the field (the wavelength of the superlong wave photon), and $\overline{H_\lambda^2}$ is the mean-square value of the field intensity

It should be noted that within the framework of formula (1), i.e., without allowance for the motion of the medium, the energy density E_λ does not depend on the electric conductivity σ. Thus, in the given approximation, the energy density E_λ is the same in an electrically-conducting medium, a dielectric, or vacuum. The role of the electric conductivity becomes significant if the motion of the medium is taken into account.

Allowance for the motion of the medium greatly complicates the problem. However, at a large value of the electric conductivity, $\sigma \gg 1$, and also in the case of turbulent isotropic motion of the plasma, the formulas for the determination of the spectral distribution of the energy or the average strength of the magnetic field can be obtained in the following form:

$$E_\lambda\, d\lambda = \frac{1}{8\pi}\overline{H_\lambda^2}\, d\lambda = kT\exp\left[\frac{\overline{v^2}}{c^2}\frac{\sigma}{\tau}\alpha(\lambda)\right]\frac{d\lambda}{\lambda^4}, \qquad (2a)$$

$$E = \int_{\lambda_0}^{\infty} E_\lambda\, d\lambda = \frac{kT}{3}\exp\left[\frac{\overline{v^2}}{c^2}\frac{\sigma}{\tau}\alpha(\lambda)\right]\frac{1}{\lambda^3} \quad (\infty > \lambda \geqslant \lambda_0), \qquad (2b)$$

where $\overline{v^2}$ is the mean-squared velocity of the medium, τ is a certain quantity with the dimension of time (it characterizes the attenuation of the turbulent motion), $\alpha(\lambda)$ is a certain function on the order of unity and varies slowly with λ, and λ_0 is the wavelength that determines the wavelength interval in which formulas (2) can be employed (the function $\alpha(\lambda)$ is almost constant and is larger than zero).

In order of magnitude, we can write

$$\overline{v^2} = 10^5 - 10^7 \text{ cm/sec}, \quad T = 10^6 - 10^7 \text{ (in star)},$$
$$\sigma = 10^{16} - 10^{18} \text{ sec}^{-1}, \quad \tau = 10^7 - 10^9 \text{ sec},$$
$$\lambda_0 = 10^5 - 10^{10} \text{ cm}, \quad \alpha(\lambda) = 1.$$

Depending on the concrete values of the parameters $\overline{v^2}$, σ, etc., E_λ and E can, in accordance with formulas (2a) and (2b), be quite large. Thus, for example, at quite acceptable values of the indicated parameters we can obtain for $(\overline{H_\lambda^2})^{1/2}$, i.e., for the mean value of the magnetic field intensity, values on the order of several Gauss and more.

However, a more accurate calculation of $\overline{H_\lambda^2}$ calls for a determination of the function $\alpha(\lambda)$. In view of the technical difficulties in solving this problem, it is advantageous to perform the calculations with an electronic computer.

V. A. Akulichev, L. R. Gabrilov, V. G. Grebinnik, V. A. Zhukov, G. Libman (East Germany), A. P. Manych, L. D. Rozenberg (deceased), Yu. I. Rudin, and G. I. Selivanov. Influence of Ultrasound on the Formation of High-energy Particle Tracks in a Liquid-hydrogen Bubble Chamber.

The main shortcoming of the existing bubble chambers is the presence of a structurally-complicated mechanical expansion system[1], which limit the oper-

ating speed of the chambers and prevent realization of the controlled regime that is of considerable interest for the registration of rare events. Extensive research has therefore been carried out in recent years for the purpose of creating a superheated state of a liquid without using mechanical expansion systems. Several attempts were made[2-4] to reveal the sensitivity of various liquids to ionizing radiation under the influence of ultrasound, but these attempts did not lead to sufficiently clearly observable particle tracks. Finally, a recent paper[5] describes experiments in which pion and proton tracks were observed in a helium bubble chamber by producing superheat with the aid of a plane standing ultrasonic wave of frequency 110 kHz.

Independent investigations of the influence of ultrasound on the formation of high-energy particle tracks in a bubble chamber, starting with 1967, have been carried out jointly by the members of the Laboratory for Nuclear Problems (LNP) of the Joint Institute for Nuclear Research (JINR) and of the Acoustics Institute of the USSR Academy of Sciences.

The investigations were performed with the 25-cm liquid-hydrogen bubble chamber of the LNP[6], inside the working volume of which were placed an acoustic radiator and an acoustic receiver. The acoustic radiator was a cylindrical focusing system of sectionalized barium titanate ceramic, emitting ultrasonic energy at a resonant frequency corresponding to a zeroth oscillation mode equal to 14.0 kHz. The radiator was axially-symmetrically located in the central part of the chamber. The inside diameter of the radiator was 70 mm, the outside diameter 150 mm, and the depth 60 mm.

A block diagram of the experimental setup is shown in Fig. 1. The chamber was placed in the beam of 340 ± 10 MeV π^- mesons obtained from the LNP synchrocyclotron. The instant of passage of the particles through the working volume was strictly synchronized with the emission of the ultrasonic pulse, the starting of the expansion system, and the stereo photography of the working volume of the chamber.

Figure 2 shows photographs of particle tracks from the synchrocyclotron in the liquid-hydrogen bubble chamber with a magnetic field on the order of 2.5 kOe at a working temperature 27°K and an expansion reduced by a factor of two compared with the usual expansion regime. An ultrasonic pulse of duration 15 msec and voltage 1.2 kV was applied to the radiator simultaneously with the expansion-system pulse. The amplitude of the pressure of the ultrasonic pulse, producing additional superheating in the liquid, was approximately 1.0 atm.

It is easy to see that introduction of ultrasound greatly influences the growth of the track-producing bubbles. Excitation of the radiator at the frequency of the zeroth mode ensured production of such an acoustic field in the working volume of the chamber, that spatially continuous tracks were observed. The use of a focusing system has made it possible to produce in the liquid acoustic-pressure amplitudes greatly exceeding the pressure on the surface of the radiator, a factor of great importance for the reduction of parasitic boiling. The results offer evidence that the expansion system of a liquid-hydrogen bubble chamber can be completely replaced by an ultrasonic oscillating system.

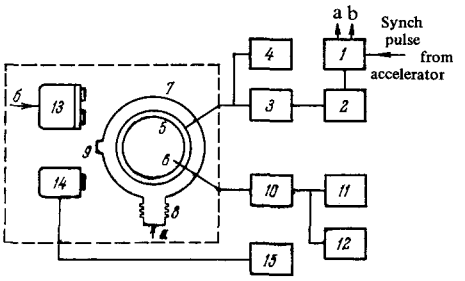

FIG. 1. Block diagram of experimental setup: 1 – bubble chamber synchronization block; 2 – pulse generator; 3 – high-power ultrasonic generator; 4 – pulsed voltmeter; 5 – acoustic radiator; 6 – pressure receiver; 7 – liquid-hydrogen bubble chamber; 8 – expansion system; 9 – beam exit window; 10 – preamplifier; 11 – oscilloscope; 12 – vacuum tube voltmeter; 13 – stereo camera; 14 – transmitting television camera; 15 – television receiver.

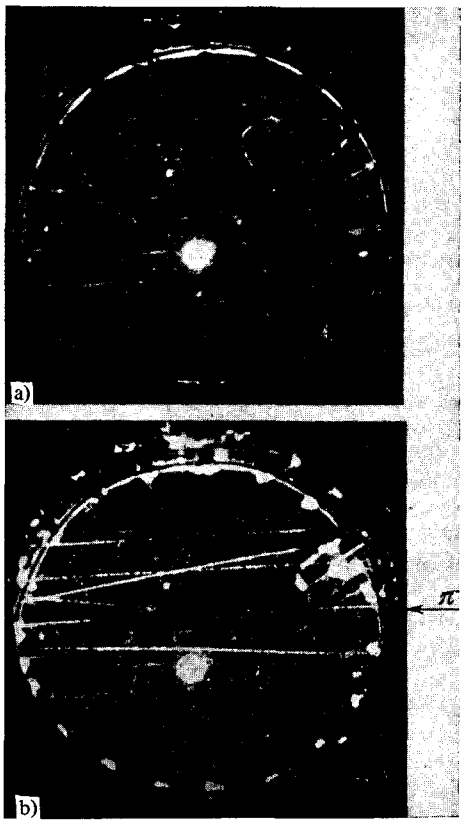

FIG. 2. Photographs of tracks of negative pions of 340 MeV energy in a liquid-hydrogen bubble chamber at a degree of expansion corresponding to the minimum sensitivity (piston travel 10 mm). The arrow indicates the direction of the particles from the synchrocyclotron: a) without ultrasound; b) with ultrasound (pulse duration – 50 msec, oscillation frequency 14.0 kHz. Radiator voltage 1.2 kV).

[1] Yu. A. Aleksandrov, G. S. Voronov, N. B. Delone, and Yu. I. Nechaev, Puzyr'kovye kamery (Bubble Chambers), Gosatomizdat, 1963.

[2] A. L. Hughes, Proc. Int. Conf. High Energy Phys., Berkeley, 1960.

[3] V. K. Lyapidevskiĭ, R. M. Sulyaev, and I. V. Falomkin, JINR Preprint No. 84, Dubna, 1962.
[4] Yu. A. Aleksandrov, G. S. Voronov, and N. B. Delone, FIAN Preprint A-151, 1962.
[5] R. C. A. Brown, H. I. Hilke, and A. H. Rogers, Nature 220, 1177 (1968).
[6] T. D. Blokhintsev, A. T. Vasilenko, V. G. Grebinnik, V. A. Zhukov, G. Libman, L. L. Nemenov, G. I. Selivanov, and Yuan Jung-fang, PTÉ No. 5, 51, (1962).

G. A. Smolenskiĭ, R. V. Pisarev, and I. G. Siniĭ, Investigation of Magnetooptic Phenomena in Ferro- and Antiferromagnets

The first magnetooptic (MO) investigations of ferro- and antiferromagnetic dielectrics were published 10 years ago, when perfect iron garnets of yttrium and rare earths, transparent in the infrared and (in the case of thin layers) in the visible region of the spectrum were synthesized. It was subsequently observed that single-crystal compounds based on divalent europium, chromium halides, and fluorides of the 3d group have good transparency in the infrared, visible, and even ultraviolet regions of the spectrum. This has led to the expansion of optical and MO investigations of magnetically-ordered compounds. MO research was greatly stimulated by the great potential capabilities of using magnetically-ordered materials for practical application in light channels for beam control (for the development of modulators, shutters, circulators, memory elements, and other devices).

The present paper is devoted to MO research carried out during the last few years in the Laboratory of Magnetism and Ferroelectricity of the Semiconductor Institute of the USSR Academy of Sciences. The research deals with the following effects produced in crystals by the passage of light: 1) along the external magnetic field—the Faraday effect (FE), or the rotation of the plane of polarization of the light, and 2) when the light propagates perpendicular to the field—the Cotton-Mouton effect (CME), or magnetic birefringence. The FE effect is linear in the magnetization and the CME is quadratic.

The investigation of the FE and the CME was carried out in a number of magnetically-ordered crystals with different types of magnetic ordering, ferrimagnets and antiferromagnets. An unexpected result was the fact that the FE and the CME in ferrimagnets and the CME in antiferromagnets are quantities of the same order (see the table), whereas in paramagnetic crystals the quadratic effects are weaker by a factor 2–3 than the linear effects. The mechanisms of the MO effects in magnetically ordered compounds were considered within the framework of the concept of the polarizability tensor. It is shown that the FE is determined by the spin-orbit interaction, and the main contribution to the CME is connected with the isotropic exchange interaction between the paramagnetic ions in different sublattices. At the same time, there should exist a contribution to the CME, due to the anisotropy of the single paramagnetic ion, and also due to the anisotropy of the exchange interaction. These two contributions can lead to the CME anisotropy, which can be appreciable in rare-earth iron garnets. The analysis of the mechanisms of these two principal MO effects is in good agreement with the results of the experimental research. Thus, for example, in the ferrimagnet RbN; F_3 (Curie point $T_C = 139°K$) at $T < T_C$, the FE and CME differ insignificantly (see the table). On going through T_C, however, the FE decreases by 1–2 orders of magnitude, whereas the decrease of the TME reaches 3–4 orders, i.e., in the paramagnetic region, where the contribution of the exchange mechanism to the CME vanishes, the usual ratio of the values of the linear and quadratic MO effects is observed.

In measurements of the CME in cubic terbium iron garnet $Tb_3Fe_5O_{12}$, a strong anisotropy of the effect was observed, which increased with decreasing temperature. Thus, at a wavelength $\lambda = 1.15\ \mu$ and $T = 295°K$, the result was $\Delta n^{100} = 6 \times 10^{-5}$, and with decreasing temperature the birefringence increased to $\Delta n^{100} = 70 \times 10^{-5}$ at 77°. Similarly, $\Delta n^{111} = 3 \times 10^{-5}$ at 295°K, and with decreasing temperature Δn^{111} reverses sign at 200°, reading $\Delta n^{111} = -72 \times 10^{-5}$ at 77°K. An analysis of the $\Delta n(H, T)$ curves shows that magnetic birefringence in $Tb_3Fe_5O_{12}$ must be connected not only with the CME, but also with birefringence due to magnetostriction, which reaches large values in this crystal. An anomaly of the birefringence was observed in the vicinity of the magnetic compensation point T_{comp}, namely a double change in the sign of the birefringence together with an increase in the depolarization and scattering of light passing through the crystal. These phenomena were observed in sufficiently strong magnetic fields and are the consequence of stimulated phase transitions from one ferromagnetic state into the antiferromagnetic state, and then into another ferromagnetic state with changing temperature. The turning of the magnetic sublattices at the compensation temperature leads to a reversal of the sign of Δn, and the fluctuation of the direction and magnitude of the magnetic moments cause an increase in the depolarization and scattering of the light.

The foregoing experiments were performed in a spectral region where the investigated crystals were

Quadratic CME and linear FE in ferromagnets and antiferromagnets (in a field H = 20 kOe)

Crystal	T_{CM}, °K	T_{expt}	λ, μ	Δn_{CM}	β_{CM} deg/cm	Δn_F	α_F deg/cm
$Y_3Fe_5O_{12}$	550	295	1,15	$4,5 \cdot 10^{-5}$	141	$1,6 \cdot 10^{-4}$	260
α-Fe_2O_3	950	295	1,15	$2,1 \cdot 10^{-4}$	657	—	—
$RbNiF_3$	139	77	0,555	$2,2 \cdot 10^{-5}$	142	$3 \cdot 10^{-5}$	95
$RbFeF_3$	102	77	0,556	$2,5 \cdot 10^{-4}$	1600	$2,2 \cdot 10^{-4}$	680
$Tb_3Fe_5O_{12}$, [100]	568	295	1,15	$6,0 \cdot 10^{-5}$	188	$2,9 \cdot 10^{-4}$	450